

## Production of optically trapped $^{87}\text{RbCs}$ Feshbach molecules

Michael P. Köppinger, Daniel J. McCarron, Daniel L. Jenkin, Peter K. Molony, Hung-Wen Cho, and Simon L. Cornish  
*Joint Quantum Centre (JQC) Durham/Newcastle, Department of Physics, Durham University, South Road,  
 Durham DH1 3LE, United Kingdom*

C. Ruth Le Sueur, Caroline L. Blackley, and Jeremy M. Hutson  
*Joint Quantum Centre (JQC) Durham/Newcastle, Department of Chemistry, Durham University, South Road,  
 Durham, DH1 3LE, United Kingdom*

(Received 12 December 2013; published 5 March 2014)

We report the production of  $^{87}\text{RbCs}$  Feshbach molecules in a crossed-beam dipole trap. A mixture of  $^{87}\text{Rb}$  and  $^{133}\text{Cs}$  is cooled close to quantum degeneracy before an interspecies Feshbach resonance at 197 G is used to associate up to  $\sim 5000$  molecules with a temperature of  $\sim 300$  nK. The molecules are confined in the dipole trap with a lifetime of 0.21(1) s, long enough for future experiments exploring optical transfer to the absolute ground state. We have measured the magnetic moment of the Feshbach molecules in a magnetic bias field range between 181 and 185 G to demonstrate the ability to control the character of the molecular state. In addition, we have performed Feshbach spectroscopy in a field range from 0 to 1200 G and located three previously unobserved resonances at high magnetic fields.

DOI: [10.1103/PhysRevA.89.033604](https://doi.org/10.1103/PhysRevA.89.033604)

PACS number(s): 67.85.-d, 31.50.Bc, 34.20.Cf

### I. INTRODUCTION

The production of ultracold polar molecules is of significant interest for a wide range of potential applications [1]. The permanent electric dipole moments of these molecules give rise to anisotropic, long-range dipole-dipole interactions which, when coupled with the precise control attainable for quantum systems, result in new prospects for research. Samples of ultracold molecules could prove useful for quantum simulation of condensed matter systems [2,3], quantum computation [4,5], precision measurements [6–10], and controlled chemistry [11,12].

Although other methods are making progress [13–16], currently the most successful technique for creating ultracold polar molecules relies on a two-step indirect method where the constituent atoms in a mixed-species quantum gas are associated into ground-state molecules [17]. First weakly bound molecules are made by magnetoassociation using an interspecies Feshbach resonance. Here, an applied magnetic field is swept across the resonance, such that the energy of the separated atomic states is tuned adiabatically through an avoided crossing with the energy of a weakly bound molecular state [18]. The molecules are then optically transferred into their rovibrational ground state by stimulated Raman adiabatic passage (STIRAP) [19]. Although this method has been successfully applied in several systems [20–22], fermionic KRb is the only polar molecule that has so far been produced at high phase-space density [20]. However, KRb is unstable as the exchange reaction  $2\text{KRb} \rightarrow \text{K}_2 + \text{Rb}_2$  is exothermic [23]. An appealing alternative is to produce ground-state RbCs which is expected to be collisionally stable because both the exchange reaction and trimer formation reactions are endothermic [24].

Pilch *et al.* [25] have investigated Feshbach resonances in  $^{87}\text{RbCs}$  at magnetic fields up to 300 G. Subsequently, Lercher *et al.* [26] achieved simultaneous  $^{87}\text{Rb}$  and Cs BECs in separated dipole traps, while McCarron *et al.* [27] achieved a dual-species BEC in a single crossed dipole trap, where a phase separation of the condensates was observed [28].

Most recently, Takekoshi *et al.* [29] extended the Feshbach spectroscopy to 667 G and reported the production of  $\sim 4000$  Feshbach molecules. They also combined information from the spectroscopy of the  $X^1\Sigma^+$  and  $a^3\Sigma^-$  molecular states with the ultracold results to obtain a precise coupled-channels model of the interaction. The interaction potentials derived for  $^{87}\text{RbCs}$  subsequently gave accurate predictions of resonance positions in  $^{85}\text{RbCs}$  by mass scaling [30].

In this paper, we report the production of up to  $\sim 5000$   $^{87}\text{RbCs}$  Feshbach molecules from a nearly quantum-degenerate sample of  $^{87}\text{Rb}$  and  $^{133}\text{Cs}$ . Molecules are trapped in an optical dipole trap with a lifetime of 0.21(1) s. We report measurements of the magnetic moment in a field range from 181 to 185 G to demonstrate the ability to control the character of the molecular state and to confirm the theoretical bound-state model. In the course of this work, we have also measured the interspecies Feshbach spectrum in a magnetic field range up to 1200 G, focusing on the previously unexplored magnetic field region above 600 G.

The structure of the paper is as follows. In Sec. II, we present the results of our work on the interspecies scattering between  $^{87}\text{Rb}$  and  $^{133}\text{Cs}$ . Calculations of the scattering length and the binding energy for weakly bound states are presented, together with our experimental observations of the Feshbach spectrum. In Sec. III, we focus on the production of  $^{87}\text{RbCs}$  Feshbach molecules and characterize the near-threshold bound-state spectrum through measurements of the magnetic moment of the molecules. In Sec. IV, we conclude with an outlook on further experiments.

### II. $^{87}\text{RbCs}$ FESHBACH SPECTRUM

#### A. Overview

The properties of a quantum-degenerate mixture are strongly influenced by both the intraspecies and the interspecies interactions [27,31–33]. As such, full knowledge of all the scattering lengths is essential when devising a strategy

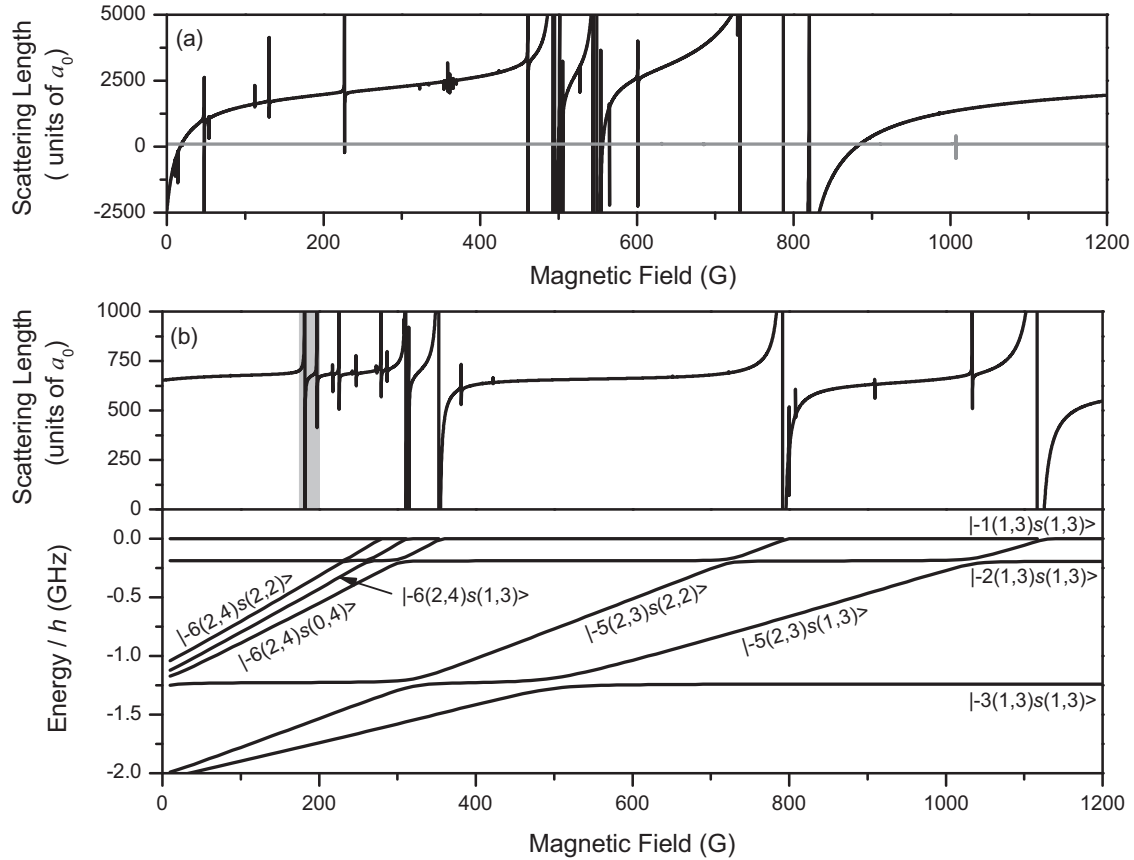


FIG. 1. (a) The intraspecies scattering length of  $^{133}\text{Cs}$  in the  $(f, m_f) = (3, +3)$  state (black) and  $^{87}\text{Rb}$  in the  $(1, +1)$  state (gray), calculated using the  $s$ ,  $d$ , and  $g$  basis functions for  $^{133}\text{Cs}$  and  $s$  and  $d$  basis functions for  $^{87}\text{Rb}$  versus magnetic field. (b) Upper panel: the interspecies scattering length between  $^{87}\text{Rb}$  and  $^{133}\text{Cs}$  in the same spin states as in (a), calculated using the  $s$  and  $d$  basis functions, versus magnetic field. The gray shaded area marks the range relevant to the magnetoassociation discussed in Sec. III and shown in Fig. 3. Lower panel: the calculated weakly bound molecular states arising from  $L = 0$  ( $s$  states). The bound-state energies are plotted relative to the energy of the lowest hyperfine state of  $^{87}\text{Rb} + ^{133}\text{Cs}$ , that is, the  $(1, +1) + (3, +3)$  hyperfine level. All the bound states shown are for  $M_{\text{tot}} = 4$ , corresponding to  $s$ -wave scattering in the lowest channel.

to produce atomic mixtures with the high phase-space densities needed for magnetoassociation. In general,  $^{87}\text{Rb}$  is a desirable constituent of a mixed-species cold-atom experiment since its scattering properties make cooling to quantum degeneracy possible over a wide magnetic field range and in several different internal states. The scattering properties of  $^{133}\text{Cs}$  are very different, exhibiting a large background scattering length and a rich spectrum of Feshbach resonances [34–37]. Efficient evaporation to Bose-Einstein condensation has been possible only in the absolute ground state ( $f = 3$ ,  $m_f = +3$ ) where inelastic two-body collisions can not occur [27,38,39]. Even in this state, efficient evaporation is possible only for moderate scattering lengths in the vicinity of the zero crossing of broad Feshbach resonances at 17.12, 556.26, and 880.90 G [37]. The intraspecies scattering lengths for  $^{87}\text{Rb}$  and  $^{133}\text{Cs}$  in their lowest hyperfine states are shown in Fig. 1(a). The  $^{133}\text{Cs}$  scattering curve is from the Supplemental Material of [37] and the  $^{87}\text{Rb}$  scattering curve was calculated using MOLSCAT [40] with the same methods outlined in [41], adjusted for the  $^{87}\text{Rb}$  parameters.

The interspecies  $s$ -wave scattering length in the lowest spin channel of  $^{87}\text{Rb} + ^{133}\text{Cs}$  in the experimentally accessible field region is shown in the top panel of Fig. 1(b). The resonance

positions and widths were calculated using MOLSCAT [40] as modified to handle collisions in magnetic fields [42], using the same basis set and methods as outlined in [29]. The parameters of the interatomic potentials were set by fitting the calculated Feshbach spectrum to experimental measurements in the field range of 0 to 600 G [25,29]. The background scattering length is  $+651(\pm 10)a_0$  associated with the existence of a least-bound state with a binding energy of  $110(2)\text{ kHz} \times h$  [29]. The bound states immediately below threshold ( $< 2\text{ GHz} \times h$ ) which are shown in the bottom panel of Fig. 1(b) were also obtained in the manner outlined in [29], using the BOUND package [43]. For the purposes of this study, all states with physical end-over-end rotation ( $L > 0$ ) were excluded to make the figure and interpretation less cluttered. As in [29], bound states are labeled as  $|n(f_{\text{Rb}}, f_{\text{Cs}})L(m_{f_{\text{Rb}}}, m_{f_{\text{Cs}}})\rangle$ , where  $n$  is the vibrational label for the particular hyperfine  $(f_{\text{Rb}}, f_{\text{Cs}})$  manifold counting down from the least-bound state which has  $n = -1$ . One additional quantum number  $M_{\text{tot}}$  is omitted because in this study its value is always 4.

The high positive value of the background interspecies atomic scattering length determines the characteristics of the ultracold mixture. It leads to large three-body losses during the cooling process, which makes it difficult to produce a

large sample of ultracold atoms at high phase-space densities suitable for magnetoassociation [26,27,44]. When quantum degeneracy is reached, it leads to a phase separation of the two condensates [28]. Fortunately, the interspecies scattering length shows many Feshbach resonances as well. The broad resonances due to  $s$ -wave states offer the possibility of improving the evaporation efficiency through tuning the interspecies collision cross section. In this context, the two previously unobserved high-field resonances at 790 and 1115 G are interesting candidates. There are also many narrower resonances on which to explore magnetoassociation of molecules.

### B. Experimental details

Details of our apparatus have been previously described in the context of studies on dual-species  $^{87}\text{Rb}$ - $^{133}\text{Cs}$  condensates [27,44] and Feshbach spectroscopy of an  $^{85}\text{Rb}$  and  $^{133}\text{Cs}$  mixture [30]. Initially cold atoms are collected in a two-species magneto-optical trap (MOT). The  $^{87}\text{Rb}$  and  $^{133}\text{Cs}$  atoms are then optically pumped into the ( $f = 1, m_f = -1$ ) and ( $3, -3$ ) states, respectively, and loaded into a magnetic quadrupole trap. The  $^{87}\text{Rb}$  atoms are then further cooled by forced rf evaporation while interspecies elastic collisions cool the  $^{133}\text{Cs}$  sympathetically. At  $40\ \mu\text{K}$ , further efficient evaporation is prevented by Majorana losses [45] and the two species are transferred into a crossed-beam dipole trap formed using a 30 W single-frequency fibre laser at 1550 nm. The crossed trap consists of two independent beams, typically up to 6 W in power, focused to waists of  $70\ \mu\text{m}$ . The beams intersect at an angle of  $22^\circ$ , at a position  $\sim 100\ \mu\text{m}$  below the field zero of the quadrupole trap. The dipole trap is loaded by simply reducing the magnetic field gradient of the quadrupole trap to  $29\ \text{G/cm}$ . Immediately following the transfer to the dipole trap, a 22 G bias field in the vertical direction is ramped on in 18 ms and rf adiabatic rapid passage is used to transfer the  $^{87}\text{Rb}$  and  $^{133}\text{Cs}$  atoms into the ( $1, +1$ ) and ( $3, +3$ ) states, respectively [46]. The bias field is added to the quadrupole field in such a way to produce a magnetic potential where the magnitude of the field increases in the upwards direction, thereby levitating the final high-field-seeking states of the atoms against gravity. The magnetic field gradient of  $29\ \text{G/cm}$  is chosen to be just below the  $30.1\ \text{G/cm}$  ( $30.5\ \text{G/cm}$ ) required to levitate  $^{87}\text{Rb}$  ( $^{133}\text{Cs}$ ) at this magnetic field in order to aid evaporation from the trap. The near-identical ratios of magnetic moment to mass for this mixture ensure excellent spatial overlap of the two species in the trap.<sup>1</sup> The dipole trap depth for  $^{133}\text{Cs}$  is  $\sim 1.4$  times deeper than that for  $^{87}\text{Rb}$  due to the different polarizabilities at 1550 nm, making the trap well suited for sympathetic cooling of  $^{133}\text{Cs}$  via the direct evaporation of  $^{87}\text{Rb}$  by decreasing the power of the dipole trap beams. The large interspecies scattering length ensures that the two species remain in thermal equilibrium. To probe the mixture, the trap and magnetic fields

are switched off and resonant absorption images are captured for both species simultaneously using a frame-transfer CCD camera [47].

Typically,  $2.8(2) \times 10^6$   $^{87}\text{Rb}$  atoms at a temperature of  $9.6(1)\ \mu\text{K}$  are confined in the dipole trap following the spin flip. The number of  $^{133}\text{Cs}$  atoms collected in the MOT is actively controlled allowing the number ratio of  $^{87}\text{Rb}$  and  $^{133}\text{Cs}$  to be varied precisely. The depth of the trap for  $^{87}\text{Rb}$  ( $^{133}\text{Cs}$ ) is then decreased from  $76\ \mu\text{K}$  ( $103\ \mu\text{K}$ ) to  $3.1\ \mu\text{K}$  ( $4.2\ \mu\text{K}$ ) over 1.25 s. The majority of the evaporation is performed at a bias field of 22 G where  $^{133}\text{Cs}$  can be cooled efficiently, although the final stages of cooling are performed at a magnetic field within the field range under investigation. Following the evaporation, a sample of typically  $\sim 5 \times 10^5$   $^{87}\text{Rb}$  atoms and  $\sim 5 \times 10^4$   $^{133}\text{Cs}$  atoms with a temperature between 200 and 700 nK remains confined in the dipole trap. Feshbach spectroscopy is then performed by exposing the ultracold atomic mixture to different magnetic bias fields and detecting the atom loss. The hold time at each field is adjusted to between 300 and 500 ms for different loss features to give the clearest signal. The significant imbalance in atom number between the two species increases the sensitivity of heteronuclear Feshbach spectroscopy; the  $^{133}\text{Cs}$  atoms act as a probe species immersed in a collisional bath of  $^{87}\text{Rb}$  atoms [48]. The magnetic field is calibrated using microwave spectroscopy between Zeeman components of the different hyperfine states of  $^{133}\text{Cs}$ . These measurements reveal the long-term reproducibility of the field to be 0.1 G in the range 0 to 400 G and 0.5 G in the range 400 to 1200 G.

### C. Results

The scattering length  $a(B)$  passes through a pole at a Feshbach resonance, and in the vicinity of the resonance may be represented  $a(B) = a_{\text{bg}} [1 - \Delta / (B - B_0)]$  [49], where  $a_{\text{bg}}$  is the background scattering length,  $B_0$  is the resonance position, and  $\Delta$  is the width. The three-body recombination rate scales approximately as  $a^4$  [50]. Typical signatures of the resonances we observe in three-body loss spectra are shown in Fig. 2 for the two resonances due to  $s$ -wave states above 600 G. In both cases, the  $^{133}\text{Cs}$  atom number shows a significant drop followed by a pronounced peak as the resonance is crossed from low to high magnetic fields. The drop in atom number is due to the increase in the recombination rate near the pole of the resonance. Fitting a Lorentzian line shape to the loss feature allows the resonance position  $B_0$  to be assigned. Conversely, near the zero crossing in the scattering length the three-body loss rate is reduced from the background value and the efficiency of sympathetic cooling improves, leading to an observed peak in the atom number. Fitting a Lorentzian line shape to the peak in atom number allows an experimental width ( $\Delta_{\text{expt}}$ ) to be determined for the resonance, defined to be the magnetic field difference between the minimum and maximum in the atom number.

In Table I, we report measurements of all five resonances due to  $s$ -wave states below 1200 G resulting from the bound-state picture shown in Fig. 1(b). For all of these resonances, we can measure an experimental width ( $\Delta_{\text{expt}}$ ). We can also calculate the width  $\Delta$  from the positions of the pole and zero crossing obtained from our coupled-channels model.

<sup>1</sup>We estimate that the small difference in magnetic moment-to-mass ratio for each species, coupled with minute unavoidable misalignments of the dipole trap beams with respect to the magnetic potential, may result in offsets between the trap centers of up to  $2\ \mu\text{m}$  in all directions. This should be compared to the cloud diameters of roughly  $90\ \mu\text{m}$  ( $460\ \mu\text{m}$ ) in the vertical (horizontal) directions.

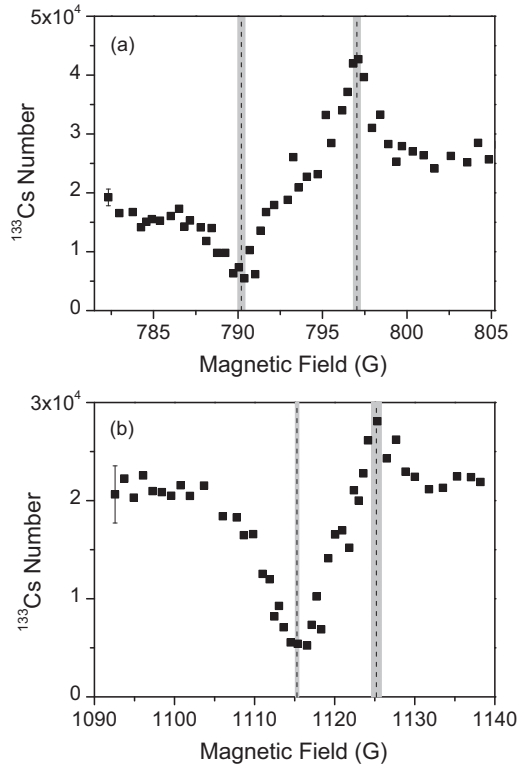


FIG. 2. Interspecies Feshbach resonances measured at (a) 790.2(2) G and (b) 1115.2(2) G. The  $^{133}\text{Cs}$  atom number shows a minimum and a maximum for each resonance. The minima define the resonance positions, while experimental widths are determined by the difference between the positions of the minima and maxima. Lorentzian fits to specific ranges of the results determine the positions. Gray shaded regions indicate the uncertainty in each position. Error bars show the standard deviations for multiple control shots at specific magnetic fields.

Ongoing theoretical work [51] suggests that the width obtained from three-body loss rates is systematically smaller than the

two-body width obtained from the pole and zero crossing in the scattering length, particularly for narrow resonances, and the present results appear to support this conclusion. In addition, we list in Table I a previously unobserved resonance due to a  $d$ -wave state at high magnetic field, together with the two resonances relevant for the magnetoassociation results presented in Sec. III. Where available, we also give the results of previous measurements [29] for comparison.

### III. MAGNETOASSOCIATION OF $^{87}\text{RbCs}$ FESHBACH MOLECULES

#### A. Overview

Feshbach molecules may be created by sweeping the applied magnetic field across a Feshbach resonance such that the energy of the separated atomic states is tuned adiabatically through an avoided crossing with the energy of a weakly bound molecular state [18]. Such a magnetoassociation sequence generally transfers a fraction of the atomic sample into the weakly bound molecular state responsible for the Feshbach resonance. The efficiency of the conversion from atoms to molecules is largely determined by the phase-space density of the atomic gas [52]. Further changes in the magnetic field allow navigation through the rich spectrum of near-threshold bound states [see the lower panel of Fig. 1(b) for example], traversing the avoided crossings between molecular states either diabatically or adiabatically depending on the rate of change of the magnetic field [53]. The molecules may be separated from the atomic cloud by exploiting the difference in the magnetic moments of the molecules and the atoms; time-of-flight expansion in the presence of an applied magnetic field gradient leads to a Stern-Gerlach separation of the atoms and molecules [54]. In bosonic gases, a fast separation is essential to minimize inelastic collisions between the atoms and molecules which lead to loss, generally associated with the molecules being transferred to more deeply bound states. Following the separation, the molecular cloud can be detected

TABLE I. Interspecies Feshbach resonances between  $^{87}\text{Rb}$  (1, +1) and  $^{133}\text{Cs}$  (3, +3) atoms. All five resonances resulting from  $s$ -wave states shown in the bound-state picture in Fig. 1(b) are reported. In addition, we list a previously unobserved resonance due to a  $d$ -wave state at high magnetic field, together with measurements of the two resonances relevant for the magnetoassociation results presented in Sec. III. This work's experimental errors shown are statistical standard errors resulting from fits as described in the text. Additional systematic uncertainties of 0.1 and 0.5 G apply to resonance positions in the field ranges 0 to 400 G and 400 to 1200 G, respectively. The results of previous measurements are listed for comparison. Theoretical widths correspond to the difference in magnetic field between the pole and zero in the scattering length.

Experiment				Theory		
This work		Previous work [29]		Quantum labels	$B_0$ (G)	$\Delta$ (G)
$B_0$ (G)	$\Delta_{\text{expt}}$ (G)	$B_0$ (G)	$\Delta_{\text{expt}}$ (G)			
Resonances due to $s$ -wave states						
279.03(1)	0.11(1)	279.12(5)	0.09(3)	$ -6(2,4)_s(2,2)\rangle$	279.020	0.034
310.72(2)	0.70(3)	310.69(6)	0.60(4)	$ -6(2,4)_s(1,3)\rangle$	310.714	0.586
352.7(2)	2.9(5)	352.65(34)	2.70(47)	$ -6(2,4)_s(0,4)\rangle$	352.744	2.218
790.2(2)	6.8(2)			$ -5(2,3)_s(2,2)\rangle$	791.791	4.227
1115.2(2)	10.0(6)			$ -5(2,3)_s(1,3)\rangle$	1116.554	8.954
Resonances due to $d$ -wave states						
181.55(5)		181.64(8)	0.27(10)	$ -6(2,4)_d(2,4)\rangle$	181.631	0.183
197.10(3)	0.1(1)	197.06(5)	0.09(1)	$ -6(2,4)_d(2,3)\rangle$	197.065	0.052
910.6(8)				$ -5(2,3)_d(1,2)\rangle$	909.345	0.006

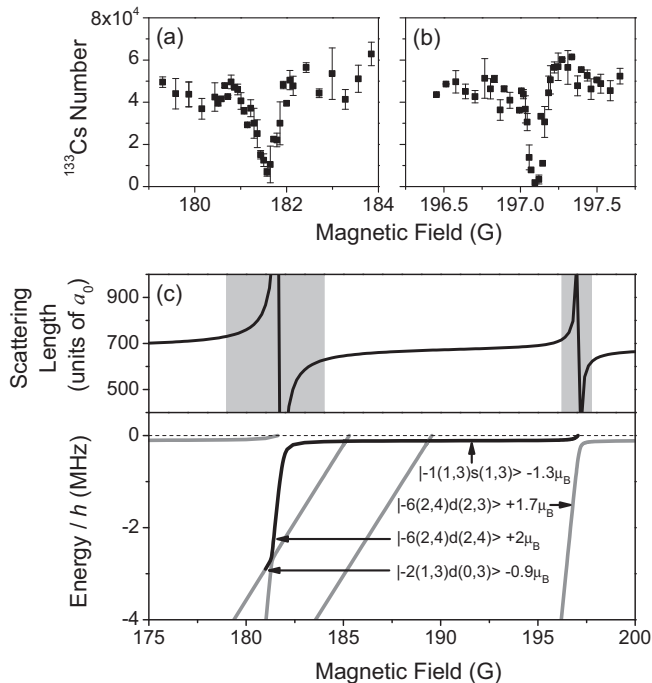


FIG. 3. The magnetoassociation sequence. The interspecies Feshbach resonances at (a) 181.55(5) G and (b) 197.10(3) G detected through loss in the  $^{133}\text{Cs}$  atom number as described in Sec. II. (c) Upper panel: the interspecies scattering length between  $^{87}\text{Rb}$  and  $^{133}\text{Cs}$  in the relevant magnetic field range. The gray shaded areas mark the field ranges shown in (a) and (b). Lower panel: the weakly bound molecular states relevant to the magnetoassociation sequence calculated using the  $s$  and  $d$  basis functions as discussed in the text. Also shown are the magnetic moments for each bound state. Molecules are produced at the Feshbach resonance at 197.10(3) G and then transferred into the  $|-2(1,3)d(0,3)\rangle$  state at 181 G following the path shown by the solid black line.

by reversing the association sequence and imaging the atoms that result from the dissociation of the molecules [55,56].

### B. Magnetoassociation sequence

The bound-state spectrum relevant to magnetoassociation of  $^{87}\text{RbCs}$  molecules is illustrated in the lower panel of Fig. 3(c). The creation and separation of molecules is complicated by the presence of the  $|-1(1,3)s(1,3)\rangle$  bound state, which runs parallel to the atomic threshold at a binding energy of 110(2) kHz  $\times h$  [29]. This state leads to strong avoided crossings just below threshold as the more deeply bound molecular states responsible for the Feshbach resonances approach threshold. As a consequence, sweeping across a Feshbach resonance from high to low field creates molecules in the near-threshold  $|-1(1,3)s(1,3)\rangle$  state with a magnetic moment of  $-1.3 \mu_B$ . Crucially, the ratio of magnetic moment to mass for molecules in this state is almost identical to that for  $^{87}\text{Rb}$  in the (1,+1) state and  $^{133}\text{Cs}$  in the (3,+3) state. Consequently, in order for the Stern-Gerlach separation to work, the molecules must be transferred into a different state with a substantially different magnetic moment. We therefore associate the molecules on the Feshbach resonance arising from the  $|-6(2,4)d(2,3)\rangle$  state at 197.10(3) G and

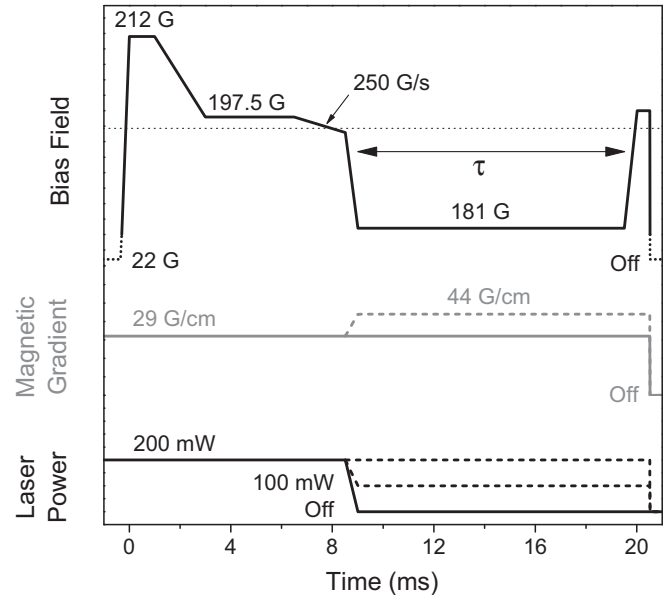


FIG. 4. The experimental sequence for the creation, Stern-Gerlach separation, and detection of Feshbach molecules. An ultracold atomic mixture is initially created by evaporation in the dipole trap at a bias field of 22 G. Subsequently, the timing sequences shown for the bias field, magnetic field gradient, and laser power in each beam of the crossed dipole trap are applied. The horizontal dotted line indicates the position of the Feshbach resonance at 197.10(3) G used for magnetoassociation. The dashed lines show the changes to routine implemented to trap the atoms in the dipole trap. The hold time  $\tau$  in the dipole trap is varied to measure the lifetime of the molecules.

then sweep the magnetic field to 181 G, adiabatically following the avoided crossing below the Feshbach resonance at 181.55(5) G and transferring the molecules via the weak-field-seeking  $|-6(2,4)d(2,4)\rangle$  state into the high-field-seeking  $|-2(1,3)d(0,3)\rangle$  state with a magnetic moment of  $-0.9 \mu_B$ . This path is illustrated in the lower panel of Fig. 3(c) by the solid black line.

The timing of the magnetoassociation sequence is shown in Fig. 4. An ultracold atomic mixture is produced by evaporation in the dipole trap at a bias field of 22 G. The magnetic field is then quickly increased to 212 G to avoid three-body losses induced by crossing several interspecies and intraspecies Feshbach resonances (see Fig. 1). From here, the field is decreased to 197.5 G, very close to the upper end of the resonance loss feature [see Fig. 3 (b)]. After a hold time of 3.5 ms to allow the magnetic field to settle, the field is further decreased by  $\sim 0.5$  G in 2 ms. During this ramp, molecules in the least-bound state  $|-1(1,3)s(1,3)\rangle$  are produced. In the current setup, the magnetic coils can levitate only high-field-seeking states against gravity. Therefore, to separate the molecules and atoms, we subsequently switch the field to 181 G in 0.1 ms, thereby transferring the molecules into the  $|-2(1,3)d(0,3)\rangle$  state. At the same time, we switch off the optical dipole trap. After 7 ms time of flight, the atoms and molecules are completely separated. To detect the molecules, the magnetic field is ramped from 181 to 199.7 G in 0.5 ms, reversing the association sequence and dissociating

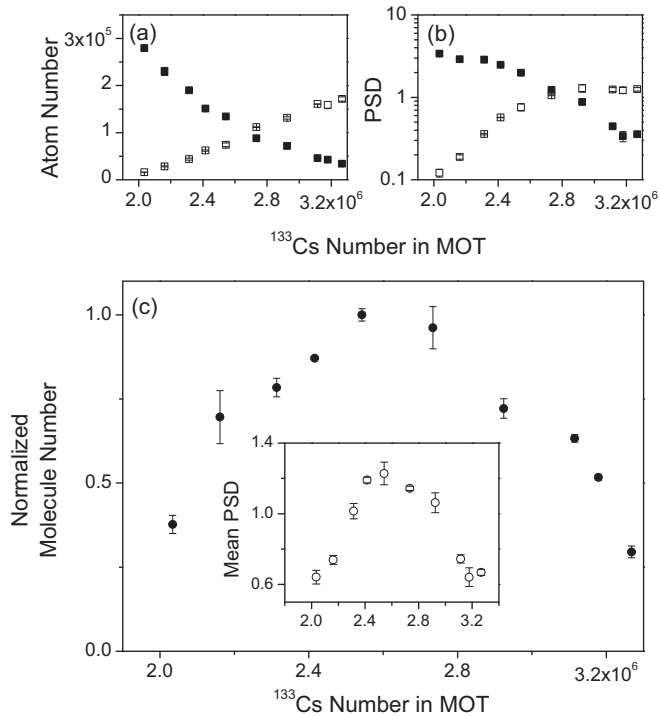


FIG. 5. Optimizing the production of Feshbach molecules by changing the composition of the initial ultracold atomic mixture. (a) Atom number and (b) peak phase-space density for <sup>87</sup>Rb (closed squares) and <sup>133</sup>Cs (open squares) at the end of a fixed evaporation sequence as a function of the number of <sup>133</sup>Cs atoms loaded into the magneto-optical trap. (c) The corresponding number of molecules produced by magnetoassociation normalized to the peak number ( $\sim 3000$  molecules in this case). The inset shows the geometric mean of the <sup>87</sup>Rb and <sup>133</sup>Cs peak phase-space densities. A strong correlation between the molecule conversion efficiency and the mean phase-space density is observed.

the molecular cloud. The magnetic bias field and gradient are then switched off and resonant absorption imaging is used to image both <sup>87</sup>Rb and <sup>133</sup>Cs onto a CCD camera.

### C. Optimizing the molecule production

The parameters of the ramp sequence reported above were all carefully optimized to maximize the number of molecules produced. The most sensitive parameter affecting the molecule production proved to be the composition of the initial ultracold atomic mixture. To explore this systematically, we varied the ratio of <sup>87</sup>Rb and <sup>133</sup>Cs by changing the number of <sup>133</sup>Cs atoms loaded into the MOT. The results are shown in Fig. 5. The performance of the evaporation sequence is extremely sensitive to the initial number of <sup>133</sup>Cs atoms loaded into the MOT. Figures 5(a) and 5(b) show that, for a fixed evaporation ramp, a 50% change in the <sup>133</sup>Cs atom number results in an order-of-magnitude change in the number and phase-space density of both <sup>87</sup>Rb and <sup>133</sup>Cs. This follows from our reliance on sympathetic cooling of <sup>133</sup>Cs throughout the evaporation sequence. Concomitantly, there is a sharp variation in the number of <sup>87</sup>RbCs molecules produced, as shown in Fig. 5(c). The molecular conversion efficiency closely follows the geometric mean of the <sup>87</sup>Rb and <sup>133</sup>Cs peak

phase-space densities, as shown in the inset of Fig. 5(c). At the peak of the plot we produce about 3000 molecules from an ultracold mixture containing  $\sim 1 \times 10^5$  atoms of each species at a temperature of  $0.1 \mu\text{K}$ . Changing the end point of the evaporation and adjusting the number of <sup>133</sup>Cs atoms loaded into the MOT to maximize the average phase-space density leads to the production of slightly more molecules. Under optimum conditions, we observe up to  $\sim 5000$  molecules produced from a sample of  $2 \times 10^5$  atoms of each species at a temperature of  $0.3 \mu\text{K}$ . This represents a conversion efficiency of  $\sim 2.5\%$ .

### D. Towards ground-state molecules

For future experiments exploring the optical transfer of the molecules to the rovibrational ground state of the singlet potential, it is desirable to confine the Feshbach molecules in the optical dipole trap. This is achieved using a slightly different experimental routine shown by the dashed lines in Fig. 4. Now, the power in the dipole trap remains on at a variable level and the magnetic field gradient is increased to  $44 \text{ G/cm}$  to levitate the molecules in the  $|-2(1,3)d(0,3)\rangle$  state. This gradient over levitates the atoms, resulting in a much reduced trap depth. Consequently, all the unconverted atoms escape from the trap within 5 ms, leaving a pure sample of molecules. To measure the lifetime of the molecules in the trap, we also reduce the power in each beam of the dipole trap to 100 mW. Under these conditions, there is no trapping potential for the atoms, so that our lifetime measurements are not contaminated by residual atomic signals. The results are shown in Fig. 6. We observe a lifetime of the Feshbach molecules in the  $|-2(1,3)d(0,3)\rangle$  state of  $0.21(1) \text{ ms}$  at a trapped density of  $\sim 8 \times 10^9 \text{ cm}^{-3}$ .

We have also measured the magnetic moment of the molecules as a function of the bias field. For this measurement, Feshbach molecules in the  $|-2(1,3)d(0,3)\rangle$  state are first loaded into the dipole trap as above. After a hold time of 50 ms, the trap is switched off and the magnetic bias field and gradient

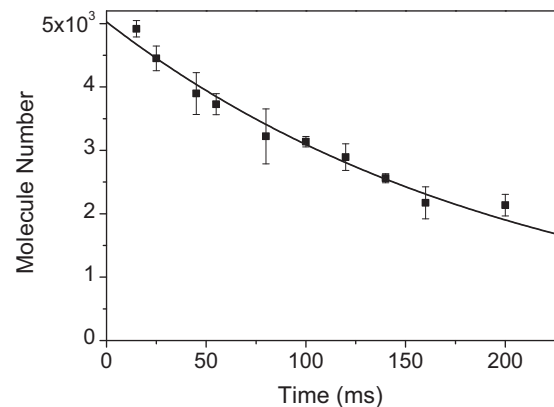


FIG. 6. Lifetime of <sup>87</sup>RbCs molecules in the  $|-2(1,3)d(0,3)\rangle$  state at 181 G held in the optical dipole trap. A magnetic field gradient of  $44 \text{ G/cm}$  is applied to levitate the molecules and the power in each beam of the dipole trap is 100 mW. Under these conditions, there is no trapping potential for the atoms. The solid line shows an exponential fit to the results, which yields a lifetime of  $0.21(1) \text{ s}$ .

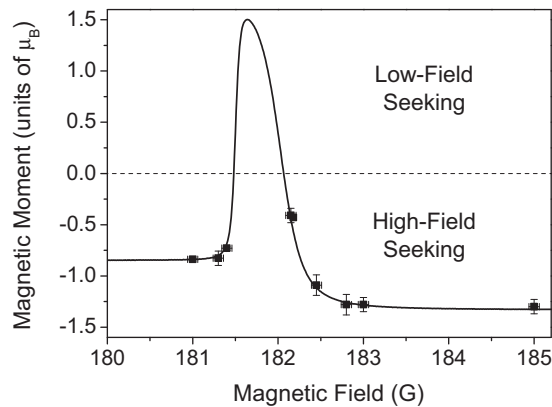


FIG. 7. Magnetic moment of the  $^{87}\text{RbCs}$  molecules as a function of the magnetic bias field. The experimental points are determined by finding the magnetic field gradient at which the molecules are levitated. Note the measurements are restricted to magnetic moments in the high-field-seeking region due to the current coil geometry in the experiment. The solid line is the theoretical prediction for the molecular states following the magnetoassociation path shown in Fig. 3(c).

are switched to different values. Measuring the magnetic field gradient at which the sample is levitated against gravity allows the magnetic moment of the molecules to be determined. The results are shown in Fig. 7 for the magnetic bias-field region between 180 and 185 G. Note that with the current coil configuration we can measure the magnetic moment of the molecules only while they are in a high-field-seeking state. The results are compared to the magnetic moment calculated from the bound-state picture shown in the lower panel of Fig. 3(c). In this plot, the zero-energy threshold corresponds to the energy of the two unbound atoms, namely,  $^{87}\text{Rb}$  in the  $(1,+1)$  state and  $^{133}\text{Cs}$  in the  $(3,+3)$  state. This energy varies with magnetic field according to the usual Breit-Rabi formula for each atom. The slope of the energy of bound states with magnetic field, taking into account the Zeeman shift of the unbound atoms, then gives the magnetic moment of the molecules. The result for the magnetoassociation path illustrated by the solid black line in Fig. 3(c) is shown by the solid line in Fig. 7. There is excellent agreement between theory and experiment. These results also demonstrate the ability to control the character

of the molecular state. Such control can be used to improve the overlap between the Feshbach molecule and electronically excited states suitable for use in optical transfer schemes to the rovibrational ground state [57].

#### IV. CONCLUSION AND OUTLOOK

In summary, we have produced ultracold samples of up to  $\sim 5000$   $^{87}\text{RbCs}$  Feshbach molecules using magnetoassociation on an interspecies Feshbach resonance. The molecules are formed from an atomic sample with a temperature of 300 nK and can be confined in an optical dipole trap with a lifetime of 0.21(1) s. We have demonstrated the control of the character of the molecules by adiabatic following of the bound-state spectrum using magnetic field ramps. The overall magnetoassociation efficiency observed in our experiment is in good agreement with results reported by Takekoshi *et al.* [29], despite very different approaches used in producing the initial ultracold atomic mixture. In the course of this work, we have also detected several previously unobserved interspecies Feshbach resonances in the high magnetic field region. The positions of these resonances agree very well with the theoretical predictions, further supporting the quality of the fitted interspecies potential [29].

These results represent a good starting point for exploring the optical transfer from the Feshbach state to the rovibrational singlet ground state using stimulated Raman adiabatic passage [19–22]. The relevant molecular spectroscopy for ground-state transfer of  $^{87}\text{RbCs}$  has recently been reported by Debatin *et al.* [58]. We have constructed a suitable laser system in which the two lasers used in the optical transfer are frequency stabilized to a common ultralow expansion optical resonator [59] and are currently investigating one- and two-photon optical spectroscopy of the ultracold  $^{87}\text{RbCs}$  Feshbach molecules. The subsequent transfer to the ground state will realize an ultracold gas of stable polar molecules with numerous applications.

#### ACKNOWLEDGMENTS

We acknowledge useful discussions with H.-C. Nägerl and members of his group and with P. S. Julienne. This work was supported by the UK EPSRC and by EOARD Grant No. FA8655-10-1-3033. C.L.B. is supported by a Doctoral Fellowship from Durham University.

- 
- [1] L. D. Carr, D. DeMille, R. V. Krems, and J. Ye, *New J. Phys.* **11**, 055049 (2009).
  - [2] A. Micheli, G. K. Brennen, and P. Zoller, *Nat. Phys.* **2**, 341 (2006).
  - [3] R. Barnett, D. Petrov, M. Lukin, and E. Demler, *Phys. Rev. Lett.* **96**, 190401 (2006).
  - [4] D. DeMille, *Phys. Rev. Lett.* **88**, 067901 (2002).
  - [5] A. André, D. DeMille, J. M. Doyle, M. D. Lukin, S. E. Maxwell, P. Rabl, R. J. Schoelkopf, and P. Zoller, *Nat. Phys.* **2**, 636 (2006).
  - [6] V. V. Flambaum and M. G. Kozlov, *Phys. Rev. Lett.* **99**, 150801 (2007).
  - [7] T. A. Isaev, S. Hoekstra, and R. Berger, *Phys. Rev. A* **82**, 052521 (2010).
  - [8] J. J. Hudson, D. M. Kara, I. J. Smallman, B. E. Sauer, M. R. Tarbutt, and E. A. Hinds, *Nature (London)* **473**, 493 (2011).
  - [9] A. E. Leanhardt, J. L. Bohn, H. Loh, P. Maletinsky, E. R. Meyer, L. C. Sinclair, R. P. Stutz, and E. A. Cornell, *J. Mol. Spectrosc.* **270**, 1 (2011).
  - [10] J. Baron, W. C. Campbell, D. DeMille, J. M. Doyle, G. Gabrielse, Y. V. Gurevich, P. W. Hess, N. R. Hutzler, E. Kirilov, I. Kozyryev, B. R. O’Leary, C. D. Panda, M. F. Parsons, E. S. Petrik, B. Spaun, A. C. Vutha, and A. D. West, *Science* **343**, 269 (2014).
  - [11] E. R. Hudson, C. Ticknor, B. C. Sawyer, C. A. Taatjes, H. J. Lewandowski, J. R. Bochinski, J. L. Bohn, and J. Ye, *Phys. Rev. A* **73**, 063404 (2006).
  - [12] R. V. Krems, *Phys. Chem. Chem. Phys.* **10**, 4079 (2008).

- [13] H. L. Bethlem and G. Meijer, *Int. Rev. Phys. Chem.* **22**, 73 (2003).
- [14] J. M. Sage, S. Sainis, T. Bergeman, and D. DeMille, *Phys. Rev. Lett.* **94**, 203001 (2005).
- [15] K. Aikawa, D. Akamatsu, M. Hayashi, K. Oasa, J. Kobayashi, P. Naidon, T. Kishimoto, M. Ueda, and S. Inouye, *Phys. Rev. Lett.* **105**, 203001 (2010).
- [16] J. F. Barry, E. S. Shuman, E. B. Norrgard, and D. DeMille, *Phys. Rev. Lett.* **108**, 103002 (2012).
- [17] B. Damski, L. Santos, E. Tiemann, M. Lewenstein, S. Kotochigova, P. Julienne, and P. Zoller, *Phys. Rev. Lett.* **90**, 110401 (2003).
- [18] C. Chin, R. Grimm, E. Tiesinga, and P. S. Julienne, *Rev. Mod. Phys.* **82**, 1225 (2010).
- [19] K. Bergmann, H. Theuer, and B. W. Shore, *Rev. Mod. Phys.* **70**, 1003 (1998).
- [20] K.-K. Ni, S. Ospelkaus, M. H. G. de Miranda, A. Pe'er, B. Neyenhuis, J. J. Zirbel, S. Kotochigova, P. S. Julienne, D. S. Jin, and J. Ye, *Science* **322**, 231 (2008).
- [21] F. Lang, K. Winkler, C. Strauss, R. Grimm, and J. Hecker Denschlag, *Phys. Rev. Lett.* **101**, 133005 (2008).
- [22] J. G. Danzl, M. J. Mark, E. Haller, M. Gustavsson, R. Hart, J. Aldegunde, J. M. Hutson, and H.-C. Nägerl, *Nat. Phys.* **6**, 265 (2010).
- [23] S. Ospelkaus, K.-K. Ni, D. Wang, M. H. G. de Miranda, B. Neyenhuis, G. Quémener, P. S. Julienne, J. L. Bohn, D. S. Jin, and J. Ye, *Science* **327**, 853 (2010).
- [24] P. S. Żuchowski and J. M. Hutson, *Phys. Rev. A* **81**, 060703(R) (2010).
- [25] K. Pilch, A. D. Lange, A. Prantner, G. Kerner, F. Ferlaino, H.-C. Nägerl, and R. Grimm, *Phys. Rev. A* **79**, 042718 (2009).
- [26] A. D. Lercher, T. Takekoshi, M. Debatin, B. Schuster, R. Rameshan, F. Ferlaino, R. Grimm, and H.-C. Nägerl, *Eur. Phys. J. D* **65**, 3 (2011).
- [27] D. J. McCarron, H. W. Cho, D. L. Jenkin, M. P. Köppinger, and S. L. Cornish, *Phys. Rev. A* **84**, 011603 (2011).
- [28] R. W. Pattinson, T. P. Billam, S. A. Gardiner, D. J. McCarron, H. W. Cho, S. L. Cornish, N. G. Parker, and N. P. Proukakis, *Phys. Rev. A* **87**, 013625 (2013).
- [29] T. Takekoshi, M. Debatin, R. Rameshan, F. Ferlaino, R. Grimm, H.-C. Nägerl, C. R. Le Sueur, J. M. Hutson, P. S. Julienne, S. Kotochigova, and E. Tiemann, *Phys. Rev. A* **85**, 032506 (2012).
- [30] H.-W. Cho, D. J. McCarron, M. P. Köppinger, D. L. Jenkin, K. L. Butler, P. S. Julienne, C. L. Blackley, C. R. Le Sueur, J. M. Hutson, and S. L. Cornish, *Phys. Rev. A* **87**, 010703 (2013).
- [31] M. R. Matthews, B. P. Anderson, P. C. Haljan, D. S. Hall, C. E. Wieman, and E. A. Cornell, *Phys. Rev. Lett.* **83**, 2498 (1999).
- [32] S. B. Papp, J. M. Pino, and C. E. Wieman, *Phys. Rev. Lett.* **101**, 040402 (2008).
- [33] C. Becker, S. Stellmer, P. Soltan-Panahi, S. Dorscher, M. Baumert, E. M. Richter, J. Kronjäger, K. Bongs, and K. Sengstock, *Nat. Phys.* **4**, 496 (2008).
- [34] P. J. Leo, C. J. Williams, and P. S. Julienne, *Phys. Rev. Lett.* **85**, 2721 (2000).
- [35] C. Chin, V. Vuletić, A. J. Kerman, and S. Chu, *Phys. Rev. Lett.* **85**, 2717 (2000).
- [36] C. Chin, V. Vuletić, A. J. Kerman, S. Chu, E. Tiesinga, P. J. Leo, and C. J. Williams, *Phys. Rev. A* **70**, 032701 (2004).
- [37] M. Berninger, A. Zenesini, B. Huang, W. Harm, H.-C. Nägerl, F. Ferlaino, R. Grimm, P. S. Julienne, and J. M. Hutson, *Phys. Rev. A* **87**, 032517 (2013).
- [38] T. Weber, J. Herbig, M. Mark, H. C. Nägerl, and R. Grimm, *Science* **299**, 232 (2003).
- [39] C.-L. Hung, X. Zhang, N. Gemelke, and C. Chin, *Phys. Rev. A* **78**, 011604 (2008).
- [40] J. M. Hutson and S. Green, MOLSCAT computer program, version 14, distributed by Collaborative Computational Project No. 6 of the UK Engineering and Physical Sciences Research Council (1994).
- [41] C. L. Blackley, C. R. Le Sueur, J. M. Hutson, D. J. McCarron, M. P. Köppinger, H.-W. Cho, D. L. Jenkin, and S. L. Cornish, *Phys. Rev. A* **87**, 033611 (2013).
- [42] J. M. Hutson, FIELD computer program, version 1 (2011).
- [43] J. M. Hutson, BOUND computer program, version 5, distributed by Collaborative Computational Project No. 6 of the UK Engineering and Physical Sciences Research Council (1993).
- [44] H. W. Cho, D. J. McCarron, D. L. Jenkin, M. P. Köppinger, and S. L. Cornish, *Eur. Phys. J. D* **65**, 125 (2011).
- [45] Y.-J. Lin, A. R. Perry, R. L. Compton, I. B. Spielman, and J. V. Porto, *Phys. Rev. A* **79**, 063631 (2009).
- [46] D. L. Jenkin, D. J. McCarron, M. P. Köppinger, H. W. Cho, S. A. Hopkins, and S. L. Cornish, *Eur. Phys. J. D* **65**, 11 (2011).
- [47] M. L. Harris, P. Tierney, and S. L. Cornish, *J. Phys. B: At., Mol. Opt. Phys.* **41**, 035303 (2008).
- [48] E. Wille, F. M. Spiegelhalder, G. Kerner, D. Naik, A. Trenkwalder, G. Hendl, F. Schreck, R. Grimm, T. G. Tiecke, J. T. M. Walraven, S. J. J. M. F. Kokkelmans, E. Tiesinga, and P. S. Julienne, *Phys. Rev. Lett.* **100**, 053201 (2008).
- [49] A. J. Moerdijk, B. J. Verhaar, and A. Axelsson, *Phys. Rev. A* **51**, 4852 (1995).
- [50] P. O. Fedichev, M. W. Reynolds, and G. V. Shlyapnikov, *Phys. Rev. Lett.* **77**, 2921 (1996).
- [51] Y. Wang and P. S. Julienne (private communication).
- [52] E. Hodby, S. T. Thompson, C. A. Regal, M. Greiner, A. C. Wilson, D. S. Jin, E. A. Cornell, and C. E. Wieman, *Phys. Rev. Lett.* **94**, 120402 (2005).
- [53] M. Mark, F. Ferlaino, S. Knoop, J. G. Danzl, T. Kraemer, C. Chin, H.-C. Nägerl, and R. Grimm, *Phys. Rev. A* **76**, 042514 (2007).
- [54] J. Herbig, T. Kraemer, M. Mark, T. Weber, C. Chin, H. C. Nägerl, and R. Grimm, *Science* **301**, 1510 (2003).
- [55] T. Mukaiyama, J. R. Abo-Shaeer, K. Xu, J. K. Chin, and W. Ketterle, *Phys. Rev. Lett.* **92**, 180402 (2004).
- [56] S. Dürr, T. Volz, and G. Rempe, *Phys. Rev. A* **70**, 031601 (2004).
- [57] J. G. Danzl, E. Haller, M. Gustavsson, M. J. Mark, R. Hart, N. Bouloufa, O. Dulieu, H. Ritsch, and H.-C. Nägerl, *Science* **321**, 1062 (2008).
- [58] M. Debatin, T. Takekoshi, R. Rameshan, L. Reichsöllner, F. Ferlaino, R. Grimm, R. Vexiau, N. Bouloufa, O. Dulieu, and H.-C. Nägerl, *Phys. Chem. Chem. Phys.* **13**, 18926 (2011).
- [59] K. Aikawa, J. Kobayashi, K. Oasa, T. Kishimoto, M. Ueda, and S. Inouye, *Opt. Express* **19**, 14479 (2011).